Materials Today: Proceedings 56 (2022) 726–734

Contents lists available at ScienceDirect

Materials Today: Proceedings

journal homepage: www.elsevier.com/locate/matpr

New Concept-Based Six-Wheels Rocker-Bogie Robot: Design and analysis

Anish Pandey [a,*], Ashwani Kumar [a], Tarun Dhar Diwan [b], Md. Ehtesham Hasan [a], Rajiva Lochan Mohanty [a], Surjeet Singh Gour [a]

[a] Kalinga Institute of Industrial Technology University, Bhubaneshwar, Odisha 751024, India
[b] Government E. Raghvendra Rao Science College, Bilaspur 751024, India

ARTICLE INFO

Article history:
Available online 23 February 2022

Keywords:
Autonomous robot
Rocker-bogie
Uneven surface
Wheels
Simulation

ABSTRACT

In the last decay, various missions have conducted to explore the science behind the space phenomenon. An autonomous robot is essential for space exploration, such as Moon, Mars, and Saturn. This robot-like rover plays a vital role in collecting data and sample on the planet's unplanned surface. This paper presents the necessary kinematic and dynamic stability of rocker-bogie on an uneven surface. The concept of a designed rocker-bogie robot ensures a new technique for optimum stability conditions of rocker-bogie and self-adaptability using a link mechanism during high-speed mode operation. It consists of a two-mode operations system with six wheels. The rocker-bogie wheels are aligned with the bar link mechanism. The two-mode operation system mechanism of rocker-bogie is simulated. Further on, the prototype of rocker-bogie is designed and fabricated by considering optimum fittest data from the simulation. The performance evaluation of the developed prototype and results is then compared with simulation aiming to strengthen vehicle stability. The newness of this present investigation are: - (i) the improvement of travel rate of rocker-bogie in case of planner surface by switching the front span from its original configure, (ii) dynamical suspension having two operational, (iii) expansion of supported polygon for increasing the travel rate in case of plane terrain, (iv) self-switching to its original configuration at low speed while it faces rough terrain.

Selection and peer-review under responsibility of the scientific committee of the International Conference on Materials, Mechanics & Modelling.

1. Introduction

Over the last decade, researches on wheeled robots are increased. Robot plays a vital role, and versatile application in many industries like defense, space, marine, medical, manufacturing unit, etc. Presently, scientists and researchers are focusing on exploration on a planetary surface. They are looking for a vehicle/wheeled robot with a high degree of freedom, high kinematic, and dynamic stability to carry out the instruction and perform the desired assignment on a planetary surface. To overcome these challenges, and appropriate robotic vehicle called rover to be necessary for planetary exploration over the last decay, the rocker-bogie used by NASA, four parallel bogies rover used by ASL, three parallel bogies with no differential mechanism used by RCL. The contact between the surface and wheel of rocker-bogie describes the helicoidal vector field by resolving the component of three traction forces [1].

Normal and weight are operated based on rover electrical and mechanical design and depend on the manipulation and navigation algorithms in outdoor rover testing [2]. The rover can spot and stay away from rock and higher gradient in an environment having unmodelled on the planetary surface [3]. The choice of optimized navigated path and controlling a rover during the uneven ground or off-road depends on the quadruped and forward motion with the rover's on-board weight. The rover's six wheels support the rover's weight, and at least rover's one wheel should be contacted with the ground surface. The understanding of wheel-soil interaction is vital for traction [4]. We can provide more stability to the rover in rocky surfaces using the gyro base technique (Kalman differential). This gyro base technique contains sun sensors and accelerometers to detect and collect accurate wheel-soil interaction [5]. Based on communication, we can control the slip of the rover wheel, and NASA did that experiment. The on-board sensors

* Corresponding author.
E-mail address: anish06353@gmail.com (A. Pandey).

https://doi.org/10.1016/j.matpr.2022.02.243
2214-7853/
Selection and peer-review under responsibility of the scientific committee of the International Conference on Materials, Mechanics & Modelling.

Nomenclature

l_i	Length of i^{th} link (i = 1, 2, 3, 4)
$\overrightarrow{V_i}$	Linear velocity i^{th} wheel(i = 1, 2, 3)
ω_1	Rotational velocity or Angular velocity of rocker-bogie
ω_2	Rotational velocity or Angular velocity of bogie
r_i	Radius of i^{th} wheel (i = 1, 2, 3)
θ	Wheel rotation
v	Effective travel speed
$r(\dot{\theta})$	Velocity due to wheel rotation
T_i	Traction force of i^{th} wheel(i = 1, 2, 3, 4, 5, 6)
Y_i	Contact angle at i^{th} wheel with surface (i = 1, 2, 3, 4, 5, 6).
θ_1	Angle between l_2 and horizontal X-axis
δ	Angle between l_2 and l_4
m_{rb}	Mass of rocker-bogie's body
Γ_i	Motor torque of i^{th} wheel (i = 1, 2, 3, 4, 5, 6)
g_{ex}	External gravity other than the earth gravity (g)
$\overrightarrow{v_D}$	Velocity of wheel D
$\overrightarrow{v_B}$	Velocity of wheel B
V_{w1}	Speed of right front wheel center (m/s)
V_{c1}	Speed of the center of the contact area (m/s)
α	Orientation of rocker-bogie
β	Orientation of bogie
γ	Contact angle between wheel and ground
S	Instantaneous slip
S_{tot}	Total slip during the full test
VCV	Velocity constraint violation
$M.D_{wr}$	Measured displacement based on the wheel rotation
$E.D_{i,j}$	Effective displacement in X and Y directions
N_i	Normal force of i^{th} wheel(i = 1, 2, 3, 4, 5, 6)
M_b	Moment produce on rocker-bogie at the center of mass of bogie
θ_2	Angle between l_3 and horizontal X-Axis
m_w	Mass of wheel.
μ	Coefficient of friction
μ_i^*	Virtual coefficient of friction of i^{th} wheel (i = 1, 2, 3, 4, 5, 6)
$\overrightarrow{v_C}$	Velocity of wheel C
V	Rocker-bogie speed (m/s)

(odometer) collect data from motion sensors to estimate the change in position relative to the current situation [6]. To improve the rover's stability, the rover needs a maximum degree of freedom in X, Y, and Z directions. However, to make stability in pitch, roll, and yaw rotation, the particular type of rover configuration is required. Various methods have been studied to determine the roll, pitch, and role of a rover, but providing stability with steering angle is the most appropriate method [7]. The next big deal was the vehicle's weight, so we need such type of rover those have light in weight called LSR (Lightweight Survivable Rover). This system works based on the gear mechanism composite joint. It is also useful in both space and earthly applications [8]. This LSR also controls the torque of six wheels during the uneven surface by minimizing the slip ratio. This slip ratio is minimized by controlling the traction force and contact angle between the wheel and ground [9]. This robot applies to the mars exploration rover introduces by NASA to find the distribution of various loads and torques of the rover [10]. It makes the rovers more autonomous on rough terrain and more comfortable to collect data return to the command location. First, it was done by the four-wheel rover, which self-supervised the planetary surface by sensing the vibration between the wheel's contact and planetary surface [11].

Testing the various rovers and how much its motion was disturbed by the influence of external distribution was studied in an article [12], by considering these external disturbances as a force act on the center of the rover's mass, we can change its original path. The rover called under steering lunar has developed by the US. This method gives the best result and restrains the original motion under the influence of external disturbance [12]. Testing various rovers in real-time, we need such a type of tool that evaluates rover performance, optimized and compared the rover efficiently and quickly. The performance optimization tool is used to test a rover. It shows CRAB, and MER rocker-bogie type structure gives the batter performance while another rover like RCL-E is not set the ideal benchmark to climb the obstacle as compare to rocker-bogie type structure [13]. This rocker-bogie type rover is simulated based on the center modeling method at flat terrain and further on the uneven place [14]. This simulation result gives a better result when the suspension is added to the vehicle. It increases the capability of the vehicle to climb the obstacle. It also increases the better control of torque and energy consumption of rover based on Newton-Euler [15]. The rover's stability also depends on the rover's wheel design because this ensures the high durability and capability of the rover while climbing the obstacle. This stability of rover secures by reducing the friction coefficient slip ratio during climbing [16]. The Taguchi method is widely used for the selection of appropriate wheel design. The wheel configurations like wheel diameter, width, and surface pattern are responsible for maintaining the performance during the rover's high traveling speed. The wheel design also depends on the rover dimension and weight [17–18]. The normal force acting on the rover relies on the rover's mass and gravity on the planet. So, we have also ensured the same rigidity of a rover under earth gravity and other gravity. By choosing an appropriate wheel design, we control the wheel's damping under the soil [19]. More important than anything is energy, and it can be reduced by the friction coefficient between the motor and surface. This energy also reduces from battery consumption and torque input given to each wheel, and this energy is used to increase the longitudinal velocity of rover [20].

This paper describes how the rover can achieve the more excellent high-speed traversal stability without affecting the original configuration at the time of high-speed operation. This designed robot is a new type of six-wheel rocker-bogies with two modes of operation with the same configuration. It can switch in a high-speed setting from the original configuration. Simple configuration or original configuration is used for high uneven surfaces, moving on a soft surface or rough with more significant obstacle having the diameter less than twice the rocker-bogie wheel's diameter. On the other hand, high-speed traverse mode configuration expands its span to increase the speed and achieve more excellent stability when it moves on a hard level surface or minor irregular with small obstacles. It can change the bogie configuration by sensing the surface using an on-board sensor on rocker-bogies. Further on, in this paper, it focuses on comparing simulated results with data of prototype tested vehicles toward aiming to strengthen vehicle stability. The rest of this paper is organized as follows: - In Section 2, we describe the forward kinematic analysis of the original configuration of rocker-bogie robot. Also, we discuss the stability condition for rocker and bogie robot. In Section 3, we propose the second mode of operation in which modification will be carried out by changing the angle of span to make a polygon type structure. Moreover, in this segment, it describes the implementation of high-speed traverse mode of rocker-bogies. The analysis of replica

of rocker-bogie by simulation and verification is carried out in Section 4. Next, in Section 5, we make an experimental setup and present the snapshots of the experimental results of a designed rocker-bogie during navigation on the rocky and uneven surfaces. Finally, future work and conclusion are given in Section 6.

2. Kinematic analysis of Rocker-Bogie robot

A rocker-bogie mechanism consists of six wheels, four front wheels attached to the rocker-bogie, and two rear wheels attach to the link called a rocker. Its configuration is linked to link 1 attached to the front wheels, and link 2 is connected to the rear wheel. The ω_1 and ω_2 are velocities of two front wheel, and ω_3 for wheel 3 (rear wheel) attached to link 2. Link 1 and link 2 joint are shown in Fig. 1, and there is a joint having rotating facilities. This joint also acts as a center of mass of rocker-bogie. The link 1 fixed with the center mass of the rocker-bogie. Fig. 2 shows two front and one rear wheel of one side view of a rocker-bogie, the same configuration is presented on the left side of the rocker-bogie. For maintaining the stable condition of a rocker-bogie, all-wheel of rocker-bogie must be in contact with the ground surface. Here, we have taken seven design parameters, namely four parameters of the link dimension (l_1, l_2, l_3, l_4) and three parameters of the wheel's radii (r_1, r_2, r_3).

2.1. Velocities

We know that the velocity is different for different wheels. If the velocity of one wheel and the other wheel quit more significant indifference, it's challenging to retain the constraints motion due to a violation of slip. It is necessary to analyze the rocker-bogie's wheel velocity distribution over an uneven place or uneven terrain during the movement to avoid the risk of slip. The difference in working velocity and the necessary velocity of each wheel of a rocker-bogie leads to the risk, and this risk is assessing by the Velocity Constraint Violation (VCV). We try to minimize this difference, so we maintain the kinematic constraints of the rocker-bogie. Violating kinematic constraints means the occurrence of slip due to the violation of minimum necessary condition on an uneven surface. We always try to make a maximum degree of rocker-bogie freedom and take care of it by the only one input velocity. The one input velocity leads to the point function, and the velocity of A point concerning different inertial coordinates can be calculated through B, C, and D points. The following equations express the velocity vectors at different points: -

$$\overrightarrow{V} = R\omega \tag{1}$$

$$\overrightarrow{v_{AD}} = \overrightarrow{V_A} = \overrightarrow{v_D} + \omega_1 R_1^0(\alpha)\overrightarrow{AD} \tag{2}$$

$$\overrightarrow{v_{AB}} = \overrightarrow{V_A} = \overrightarrow{v_B} + \omega_2 R_2^0(\alpha)\overrightarrow{AB} \tag{3}$$

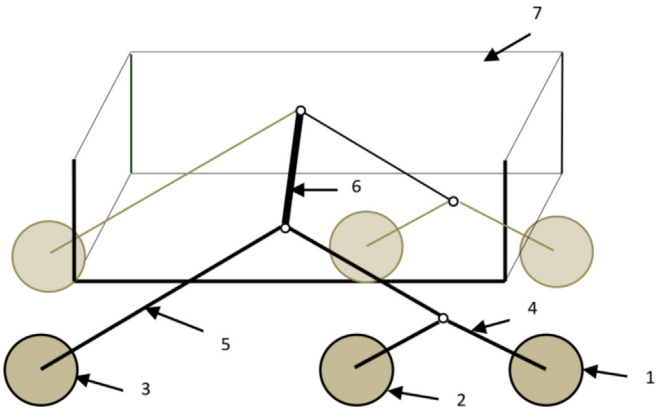

Fig. 2. Rocker-bogie system with part names: – 1. Front-wheel, 2. Middle-wheel, 3. Rear-wheel, 4. Bogie, 5. Rocker, 6. Differential mechanism, 7. Chassis.

$$\overrightarrow{v_{AC}} = \overrightarrow{V_A} = \overrightarrow{v_C} + \omega_2 R_3^0(\beta)\overrightarrow{AC} \tag{4}$$

where $R_j^i(p)$ denotes the revolution of link by angle p from i to j, $\overrightarrow{XY_i}$ is the velocity of different link in i coordinate system. The above equations can be rearranged as follows: -

$$\overrightarrow{v_{AD}} = \overrightarrow{v_{AB}} \tag{5}$$

$$\overrightarrow{v_{AD}} = \overrightarrow{v_{AC}} \tag{6}$$

By considering the motor's velocity at 'A' point, we can predict the speed at B and C points. The equation of the system can be written as an input velocity ($\overrightarrow{v_A}$), and $Ax = b$, where $x = (v_B, v_C, \omega_1, \omega_2)^T$, similarly, for the input $\overrightarrow{v}_B$ and $\overrightarrow{v}_C$.

Here the primary attention is to make a velocity as a point functions. So that velocity acted as an only input and obtained the one solution.

2.2. Slip

It is crucial to operate or define the matrix to control the slip. Based on matrix operation, we establish and differentiate the good or bad presentation of the rocker-bogie. It is done by approaching the final matrix value. The selection of an optimum value from a matrix solution is also crucial. Based on the matrix solution, we define the two types of slip. The first one occurs due to the difference in velocity value of ideal and theoretical called the instantaneous. This instantaneous slip equation can be described as follows: -

$$S = \frac{r(\dot{\theta}) - v}{r(\dot{\theta})} \tag{7}$$

The next slip is to calculate a total wheel slip occurs during the whole journey of the rocker-bogie. It is due to the difference in trac-

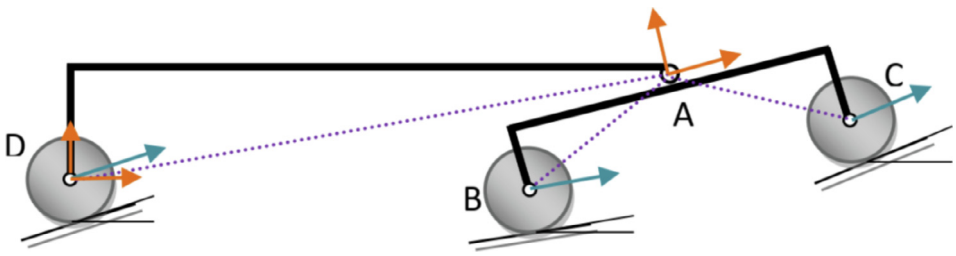

Fig. 1. Rocker-bogie wheel interaction with the ground.

tion force and friction force between the wheel's contact and surface. This type of slip is called an absolute slip, and it comprises all kinds of sliding motions. Both the slips are not suitable for the rocker-bogie because these lead to more energy and power consumption. So, it is necessary to maintain a low slip as possible for better performance.

2.3. Kinematic slip equation

For the rocker-bogie, we have to know that the parameter is the wheel's rotation and interaction with the ground during motion. There are two different methods to formulate this parameter called inverse kinematics and forward kinematics. We choose the forward kinematics to express this parameter due to its secure implant over the inverse kinematics. These also measure the overall slip of the rocker-bogie during constrain motion. The links are jointed in series with rocker-bogie frame and this rocker-bogie frame joint with each wheel. All the links have sensed the wheel's contact with the surface and maintained the constrained. The forward kinematics give the information about each wheel interaction with the ground. Besides, it provides the component of each wheel contact with the surface. The components introduced on rocker-bogie's each wheel are used to define the slip and constraints of the rocker-bogie during motion. It also provides the maximum degree of freedom of wheel concerning the ground. This degree of freedom provides more facilities in terms of a wheel velocity in different rotational motion. In reality, all correlated slip and uncorrelated slip leads to overall slip. These two slip can be determined by the decomposition of a component called deterministic constituent. The components must be none zero value comes from the result of a slip. This result has been affected by the movement of steering. The steering movement produces a turn on every and leads to yaw motion throughout the turn.

3. Analysis of straight line walking condition

3.1. Quasi-Static conditions for bogie

The linear moving condition is one of the typical and standard requirements for the automatic rocker-bogie vehicle. Under this linear moving condition, the vehicle's chassis system is powered by the motor, which transmits the power to move all the wheels. As a result, there is no axial differential device in transmission to the front and rear axles. The speed of the center of contact area between wheel and ground during sliding can be expressed as: -

$$V_{c1} = r_{m1}(w) - -v \tag{8}$$

The relationship between the shear displacement and the slip speed of the tire is a complex nonlinear. However, in the case of steady work, the X direction's displacement increases with the rise of sliding speed, which is approximately a linear relationship. In this case, the linear substitution curve is adapted to present the internal action relationship. The necessary straight-line walking condition as follow for the link l_2 and l_4. It is described in Figs. 3, 4, and 5.

$$\overrightarrow{v_{AD}} = \overrightarrow{v_{AB}} \tag{9}$$

$$\overrightarrow{v_{AD}} = \overrightarrow{v_{AC}} \tag{10}$$

$$\sum_{i=1}^{2} F_x = 0 \tag{11}$$

$$\sum_{i=1}^{2} F_z = 0 \tag{12}$$

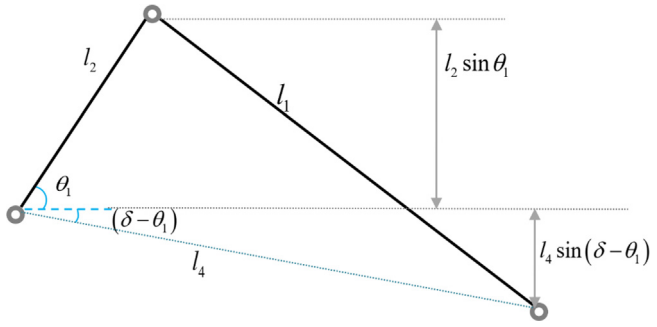

Fig. 3. Distance of link l_2 and l_4 along y-axis.

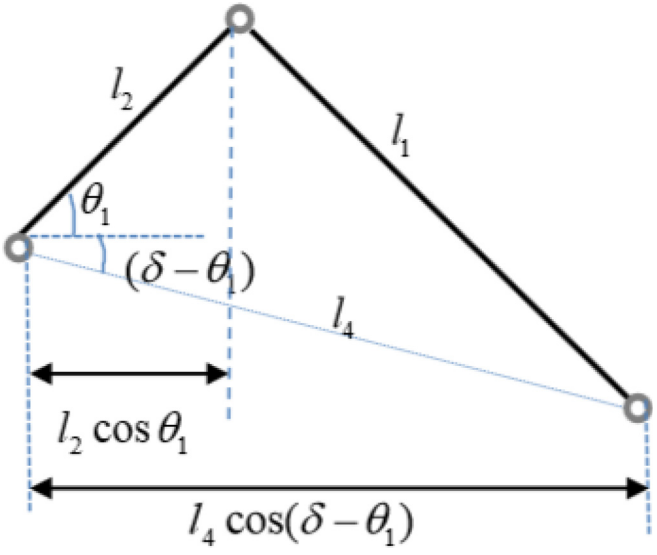

Fig. 4. Distance of link l_2 and l_4 along the x-axis.

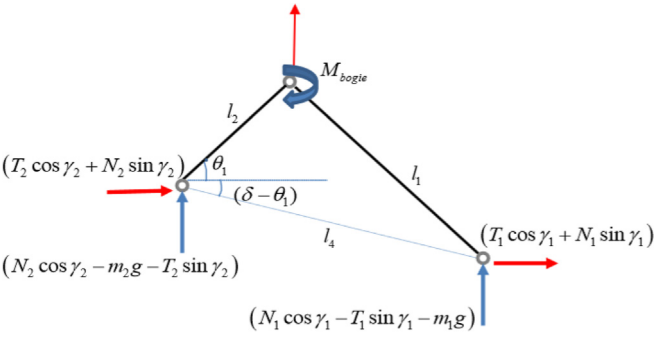

Fig. 5. Resolution of forces and moment at different junction.

$$\left\{A_x + \sum_{i=1}^{2}(T_i\cos(y_i) + N_i\sin(y_i))\right\} = 0 \tag{13}$$

$$\left\{A_z + \sum_{i=1}^{2}(T_i\cos(y_i) - N_i\sin(y_i) - m_ig)\right\} = 0 \tag{14}$$

$$\sum M_{(bogie,A)} = 0 \tag{15}$$

For quasi-static conditions, the bogie must possess the net force is zero along the X-axis and Z-axis at junction A in equations (11) and (12). Fig. 5 reveals the moment at point A, and it also represents the different components of forces at junction B and C along the X and Z direction. The net effects at points A and B must be zero, see equations (13) and (14), where A_x and A_z are reaction forces at joint A of rocker-bogie, and are against the traction forces acting on the whole rocker-bogie describe in Fig. 6.

3.2. Quasi static conditions for rocker

As shown in Fig. 7, the link l_3 is connected to point A, where the moment occurs about Y-axis. The center of mass of the whole body acts at a distance Δ from the point A. The axes where the center of mass are acting deflected by an angle θ_{change} concerning θ_2.

In the above section, the authors discuss the quasi-static condition for bogie, which must be fulfilled similarly for rocker quasi-static conditions. Rocker has a link l_3, one end of link l_3 is connected to the junction point A and other ends connected to the wheel D. At point A the component of traction force (T_3), the normal force (N_3), and wheel's weight (m_3g) is resolved in the direction of X-axis and Z-axis in Fig. 7. At a point, a moment M_{rocker} is acting along the Y-axis. It may be clockwise or anticlockwise depends upon the orientation of rocker-bogie. The bogie must pose the net force acting along the X-axis, and Z-axis is zero as well as the moment will be zero. The force and moment equations are as follows: -

$$\sum_{i=1}^{2} F_x = 0 \tag{16}$$

$$\sum_{i=1}^{2} F_z = 0 \tag{17}$$

$$-A_x + T_3\cos\gamma_3 - N_3\sin\gamma_3 = 0 \tag{18}$$

$$-A_z + T_3\sin\gamma_3 + N_3\cos\gamma_3 - (m_3 + m_b)g = 0 \tag{19}$$

$$\sum M_{(rocker,A)} = 0 \tag{20}$$

$$[(T_3\sin\gamma_3 + N_3\cos\gamma_3 - m_3g)l_3\cos\theta_2 - (T_3\cos\gamma_3 - N_3\sin\gamma_3)l_3\sin\theta_2 - m_bg(\triangle\sin\theta_{chnage}) + M_b] = 0 \tag{21}$$

As illustrated in Figs. 6 and 7, Junction A connects the rocker-bogie. For the whole rocker-bogie mechanism and the quasi-static condition, it must be satisfied the given in equations (13), 14, 18, and 19. From equations (22) and (23), the rocker-bogie mechanism decides the movement, as follows: -

$$\sum_{i=1}^{3} (N_i\cos\gamma_i - T_i\sin\gamma_i) = 0 \tag{22}$$

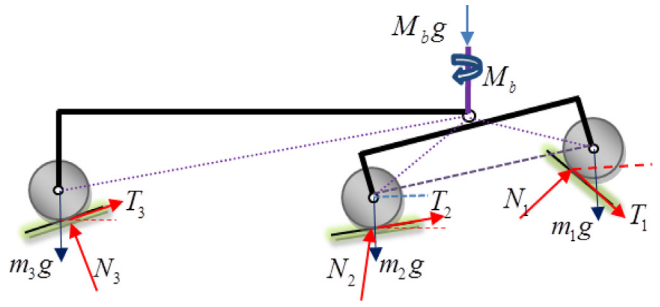

Fig. 6. All type forces and momentum acting on rocker-bogie.

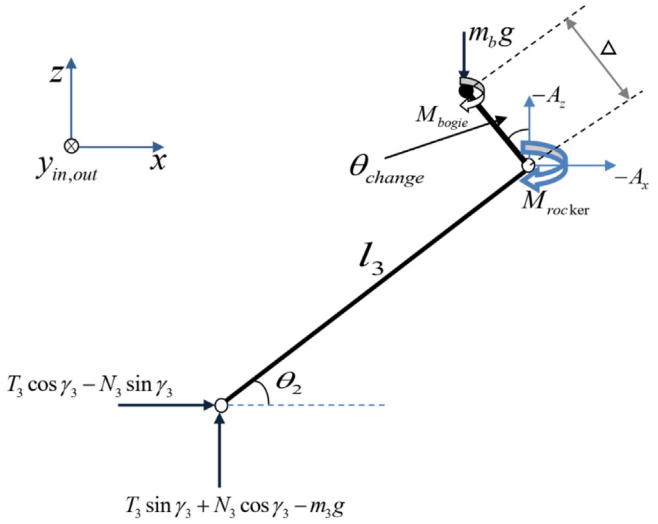

Fig. 7. Free body diagram of rocker.

$$\sum_{i=1}^{3} (N_i\sin\gamma_i + T_i\cos\gamma_i - m_ig) - m_bg = 0 \tag{23}$$

4. Brief discussion of SolidWorks model of the Rocker-Bogie robot

This section contains a brief description of the developed high speed of a two-mode rocker-bogie. The two-dimensional and three-dimensional design of two modes of rocker-bogie described using SolidWorks software. The structure of the unmanned rocker-bogie contains two units. First sensor and ranging unit that gives the idea about surrounding territory. Another unit does drive the vehicle and switch the front wheel at a certain angle called high-speed mode operation. The various components and parts have been described in Figs. 8 to 11, and part numbers and names of the different components of rocker-bogie are listed in Table 1.

The rocker-bogie consists of a rocker, bogie, wheel (4), DC motors (5), servo motors (7), DC motor clamp, servo motor clamp, bearing (6) and connecting rod (3). Similarly, the various sensors have been connected on board. Fig. 8 illustrates the isometric view of rocker-bogie. It shows the right driving wheel system consists of three-wheel. Similarly, the left driving wheel system consists of three wheels, like the front wheel, middle wheel, and back wheel, respectively. Both driving systems provide the forward, backward,

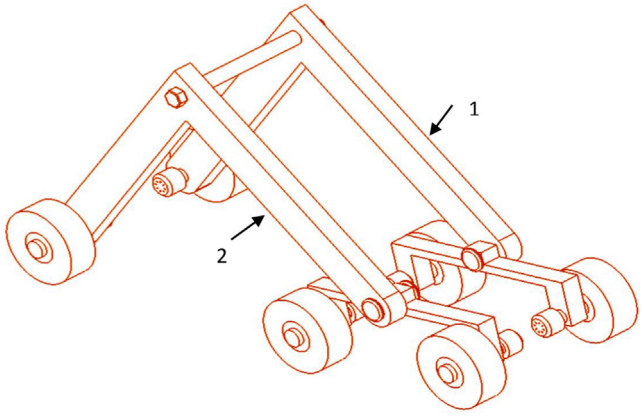

Fig. 8. Isometric view of rocker-bogie.

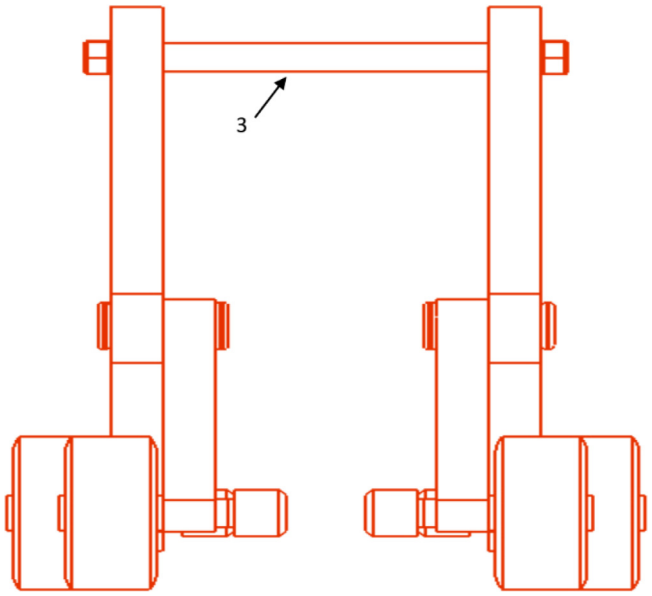

Fig. 9. Front view of rocker-bogie.

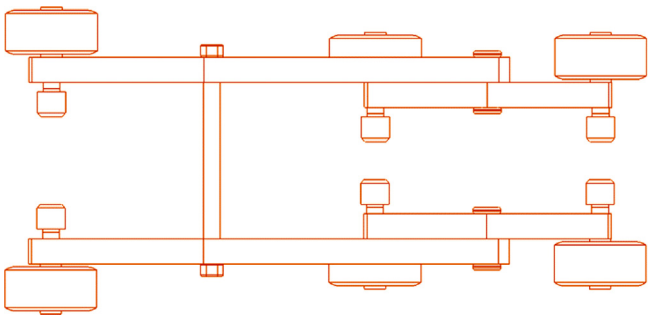

Fig. 10. Top view of rocker-bogie.

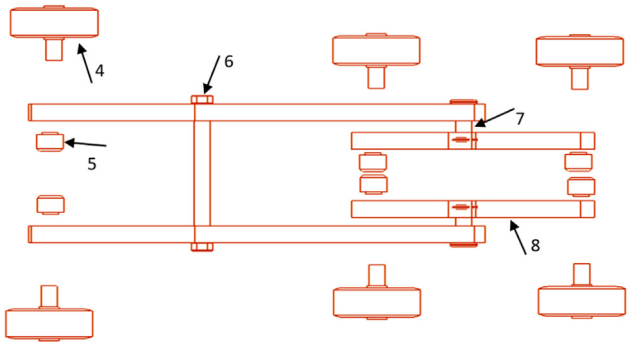

Fig. 11. Disassembled of the mechanical structure of rocker-bogie.

Table 1
Part numbers and part names of different component of rocker-bogie.

Part numbers	Part name
1	Left driving system of rocker-bogie
2	Right driving system of rocker-bogie
3	Connecting rod of rocker-bogie
4	Wheel
5	DC motor
6	Bearing
7	Servo motor
8	Bogie

clockwise, and anticlockwise motion of rocker-bogie. The next exploded view shown in Fig. 11 in the driving system has been disassembled from rocker-bogie's mechanical structure. The six DC motor connected to each wheel of rocker-bogie with the help of a motor clamp. These three sets of DC motor connected to the left driving system (1) and three sets of DC motor connected with the right driving system (2). As shown in Fig. 11, two servo motors are attached to both sides of rocker-bogie between the front leg and rocker. This servomotor provides the front wheel's switching at a certain angle in the case of a high-speed mode of the rocker-bogie and is connected with the two sides of rocker-bogie with the help of a connecting rod.

5. Experimental analysis of a Rocker-Bogie robot

This section provides the real-time experiment of a designed rocker-bogie. The snapshots of different views of the physical model of a designed rocker-bogie have been illustrated in Fig. 12 (A to E). The rocker-bogie chassis is made up of 3 mm thickness Aluminum sheet due to its high strength. Aluminum has also chosen due to it's the lightweight and robustness to the frame of the rocker-bogie. The total weight of rocker-bogie is 11 kg, length is 81 cm, width is 52 cm, and height is 38 cm. The diameter of the designed wheel is 10 cm. The rocker-bogie consists of 7 ultrasonic sensors and 2 LR sensors to move forward and the backward direction the three US sensors fixed at the front to detect the height of the obstacle.

All the commands related to kinematic equation (mentioned in the section 2) and navigation controller programs are embedded in ATmega 2500 Arduino. The entire program has been written in C and C++ languages. The IR and US sensor sends the command to the microcontroller, where the kinematics equations are verified. After the verification, the microcontroller sends the command to motor drive, and the mother drive adjusts the motion according to programs. The enable pin connected to a motor drive to control the velocity of the left and right wheel drive system of rocker-bogie. Similarly, the input pin connected to the motor drive controls the switching of front bogie into the high-speed mode and controls the clockwise and anticlockwise motion of rocker-bogie. All the command has been given to rocker-bogie through the pulse modulation. The lithium-polymer battery (LIPO) with 2000 mAh and 11.1 V governs the power to run all the DC and servo motor. And mega Arduino microcontroller uses the power form IC/7085 voltage regulator having 11.1 V to 5 V. At the front, 3 US sensors have been established. The first US sensor creates at the height equal to the wheel's radius. The second US sensor determines equally to the height of the wheel's diameter. And the third one establishes at the height of twice the wheel's diameter. When the top US sensor detects some obstacle, the sensor sends the data to the microcontroller, and the microcontroller gives the command to the motor driver to avoid this path. If the middle US sensor detects some obstacle and at the same time tops us sensor detects nothing, then rocker-bogie moves in a straight path with standard configuration. In the case of normal configuration, the rocker-bogie moves in a straight path with a speed of 1.3 m/sec. Now the third condition, when the only bottom one US sensor detects the obstacle, then microcontroller received the data and sent the command to two front servo motors. This servo motor received a command from the microcontroller and turned the front link at 21° called high-speed mode. At this mode, rocker-bogie runs at a speed of 1.6 m/sec, which quite higher than the normal mode operation because it provides better stability.

Further on, to verify the effectiveness and efficiency of the proposed rocker-bogie, we have tested this in the rocky and uneven surfaces and presented the snapshots of the experimental results

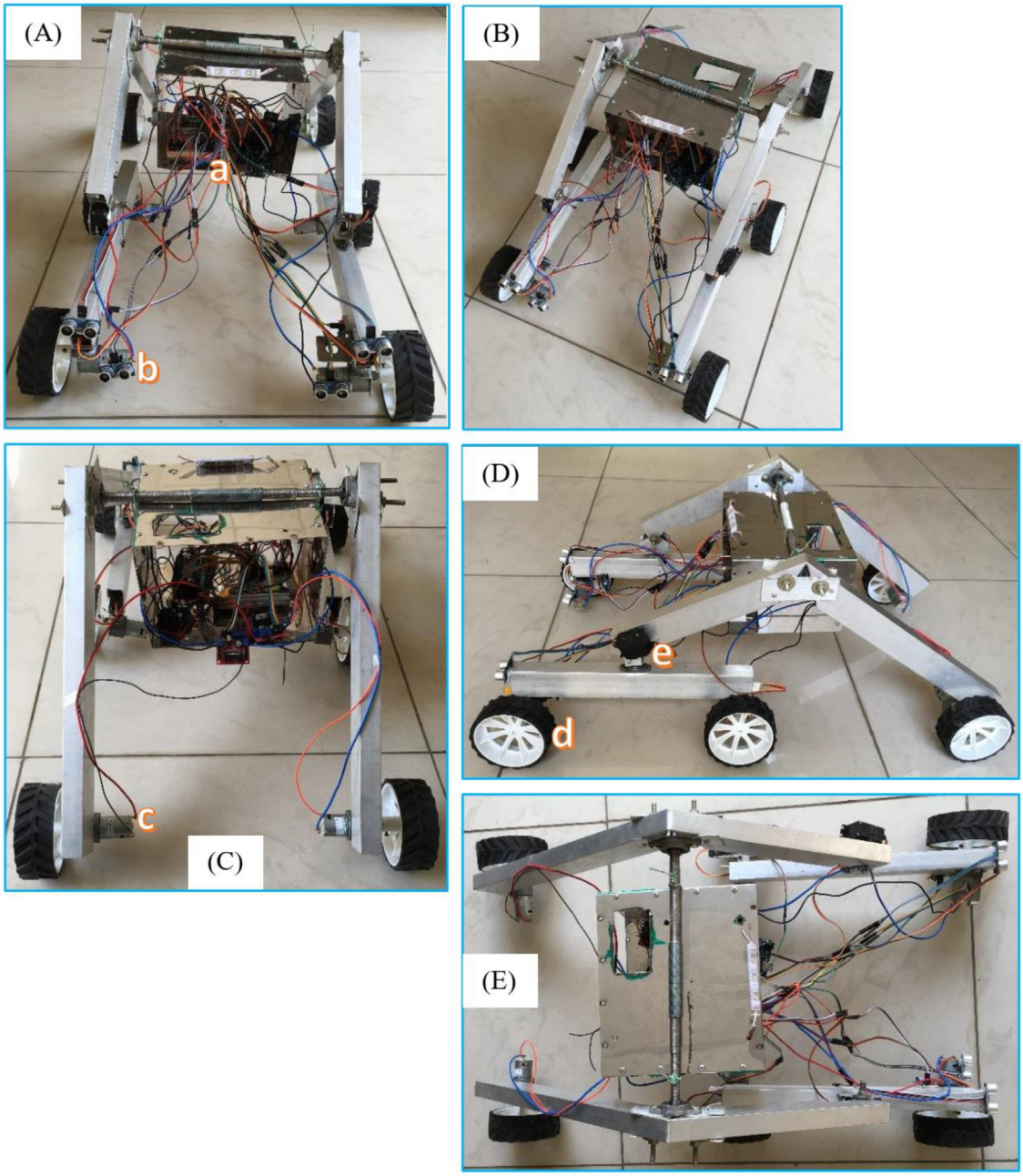

Fig. 12. Snapshots of different views of the physical model of a designed rocker-bogie: (A) Front view, (B) Isometric view, (C) Rear view, (D) Side view, (E) Top view. Note: a-Electronic box, b-Ultrasonic sensor, c-DC motor, d-Driving wheels, e-Servo motor.

during its motion in Fig. 13 (A to E). Fig. 14 reveals the real-time recorded angular velocities (in Degree/Second) of left and right driving system of rocker-bogie during navigation on the rocky and uneven surfaces in Fig. 13. In Fig. 13, it is found that the rocker-bogie successfully navigates on the rocky and uneven surfaces due to its specially designed chassis and other mechanism configurations.

6. Conclusion

In this article, we have designed and fabricated the novel concept-based six-wheels rocker-bogie robot. The proposed article's contributions are as follows: first, the mathematical kinematic equations of the rocker and bogie have been derived and presented briefly. Next, the two-dimensional and three-dimensional SolidWorks model of the rocker-bogie with part numbers and names of different components have been presented to understand the model better. Further on, real-time experimental tests have been conducted to show the developed rocker-bogie robot's effectiveness and efficiency. In the experiments, it has been found that the rocker-bogie robot successfully navigates on rocky and uneven surfaces due to its specially designed chassis and other mechanism configurations. Therefore, it can be said that this rocker-bogie robot can be used for defense purposes during searching operations in the forest and uneven terrain to carry weapons and other belongings. For future work, the solar panel with a charge con-

Fig. 13. Snapshots of the experimental results of a designed rocker-bogie during navigation on the rocky and uneven surfaces.

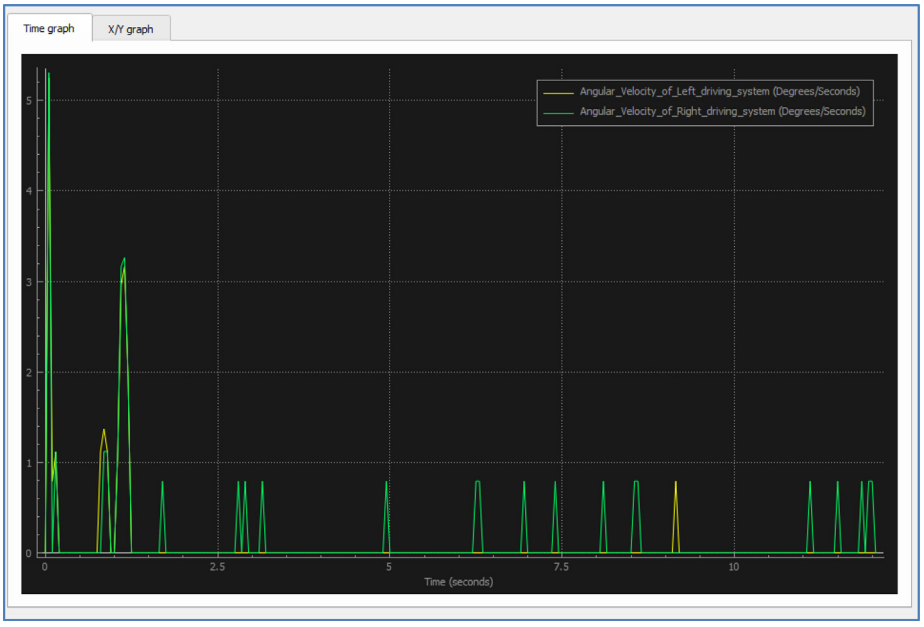

Fig. 14. Real-time recorded angular velocities (in Degree/Second) of left and right driving system of rocker-bogie during navigation on the rocky and uneven surfaces in Fig. 13.

troller can be added for the continuous power supply. The vision sensors can also be incorporated in the designed rocker-bogie robot for video surveillance during the searching operation.

CRediT authorship contribution statement

Manuscript Entitled "New Concept-Based Six-Wheels Rocker-Bogie Robot: Design and Analysis," authored by Anish Pandey, Ashwani Kumar, Tarun Dhar Diwan, Md. Ehtesham Hasan, Rajiva Lochan Mohanty, and Surjeet Singh Gour.All persons who meet authorship criteria are listed as authors, and all authors certify that they have participated sufficiently in the work to take public responsibility for the content, including participation in the concept, design, analysis, writing, or revision of the manuscript.

Declaration of Competing Interest

The authors declare that they have no known competing financial interests or personal relationships that could have appeared to influence the work reported in this paper.

References

[1] V.R. Kumar, K.J. Waldron, Force distribution in closed kinematic chains, IEEE J. Robot Automation 4 (6) (1988) 657–664, https://doi.org/10.1109/56.9303.
[2] R. Volpe, J. Balaram, T. Ohm, R. Ivlev, The rocky 7 mars rover prototype, in: Proceedings of IEEE/RSJ Int. Conf. on Int. Robo. and Sys., 1996, 1558–1564. https://doi.org/10.1109/IROS.1996.569020
[3] A.H. Mishkin, J.C. Morrison, T.T. Nguyen, H.W. Stone, B.K. Cooper, B.H. Wilcox, Experiences with operations and autonomy of the mars pathfinder microrover, IEEE Aero. Conf. Proc. (1998) 337–351, https://doi.org/10.1109/AERO.1998.687920.
[4] G. Andrade, F.B. Amar, P. Bidaud, R. Chatila, Modeling robot-soil interaction for planetary rover motion control, in: Proceedings of IEEE Int. Conf. on Intelligent Robo. and Sys. Innovations in Theory, Practice and Applications, 1998 576–581. https://doi.org/10.1109/IROS.1998.724680
[5] J. Balaram, Kinematic state estimation for a Mars rover, Robotica 18 (3) (2000) 251–262, https://doi.org/10.1017/S0263574799002234.
[6] J. Balaram, Kinematic observers for articulated rovers, in: Proceedings of IEEE Int. Conf. on Rob. and Auto., 2000 2597–2604. https://doi.org/10.1109/ROBOT.2000.846419
[7] M. Tarokh, G. McDermott, S. Hayati, J. Hung, Kinematic modeling of a high mobility Mars rover, in: Proceedings of IEEE Int. Con. on Rob. and Auto., 1999 992–998. https://doi.org/10.1109/ROBOT.1999.772441
[8] M. Bajracharya, M.W. Maimone, D. Helmick, Autonomy for mars rovers: Past, present, and future, Computer 41 (12) (2008) 44–50, https://doi.org/10.1109/MC.2008.479.
[9] T. Thueer, A. Krebs, R. Siegwart, Comprehensive locomotion performance evaluation of all-terrain robots, in: Proceedings of IEEE/RSJ Int. Conf. on Intel. Robo and Sys., 2006 4260–4265. https://doi.org/10.1109/IROS.2006.281954
[10] C.A. Brooks, K.D. Iagnemma, Self-supervised classification for planetary rover terrain sensing, in: Proc. of IEEE Aero. Conf., 2007 1–9. https://doi.org/10.1109/AERO.2007.352693
[11] K. Gu, H. Wang, M. Zhao, The analyse of the influence of external disturbance on the motion of a six-wheeled lunar rover, in: Proc. of Int. Conf. on Mechatronics and Auto., 2007 393–398. https://doi.org/10.1109/ICMA.2007.4303575
[12] T. Thueer, A. Krebs, R. Siegwart, P. Lamon, Performance comparison of rough-terrain robots simulation and hardware, J. Field Robot 24 (3) (2007) 251–271, https://doi.org/10.1002/rob.20185.
[13] Y. Chang, S. Ma, H. Wang, D. Tan, A kinematic modeling method for a wheeled mobile robot, in: Proceedings of Int. Conf. on Mechatronics and Auto., 2009 1100–1105. https://doi.org/10.1109/ICMA.2009.5246109
[14] A. Krebs, F. Risch, T. Thueer, J. Maye, C. Pradalier, R. Siegwart, Rover control based on an optimal torque distribution-Application to 6 motorized wheels passive rover, in: Proceedings of Int. Conf. on Intelligent Robots and Systems, 2010 4372–4377. https://doi.org/10.1109/IROS.2010.5653707
[15] D. Choi, Y. Kim, S. Jung, H.S. Kim, J. Kim, Improvement of step-climbing capability of a new mobile robot RHyMo via kineto-static analysis, Mech. Mach. Theory 114 (2017) 20–37, https://doi.org/10.1016/j.mechmachtheory.2017.03.018.
[16] M. Sutoh, J. Yusa, T. Ito, K. Nagatani, K. Yoshida, Traveling performance evaluation of planetary rovers on loose soil, J. Field Robot 29 (4) (2012) 648–662, https://doi.org/10.1002/rob.21405.
[17] H.S. Hong, T. Seo, D. Kim, S. Kim, J. Kim, Optimal design of hand-carrying rocker-bogie mechanism for stair climbing, J. Mech. Sci. Tech. 27 (1) (2013) 125–132, https://doi.org/10.1007/s12206-012-1212-y.
[18] H. Nakashima, T. Kobayashi, Effects of gravity on rigid rover wheel sinkage and motion resistance assessed using two-dimensional discrete element method, J. Terra. 53 (2014) 37–45, https://doi.org/10.1016/j.jterra.2014.03.004.
[19] S. Tashakori, S. Kasiri Bidhendi, B. Mashadi, J. Marzbanrad, Trajectory control and sensitivity analysis of curiosity rover on uneven terrains, J. Dyn. Sys., Meas., and Cont. 141 (11) (2019) 111001–111013, https://doi.org/10.1115/1.4043910.
[20] S. Wang, Y. Li, Dynamic rocker-bogie: kinematical analysis in a high-speed traversal stability enhancement, Int. J. Aero. Eng. 5181097 (2016) 1–8, https://doi.org/10.1155/2016/5181097.